

Molecular dynamics simulations of thermally activated edge dislocation unpinning from voids in α -Fe

J. Byggmästar,* F. Granberg, and K. Nordlund

Department of Physics, P.O. Box 43, FI-00014 University of Helsinki, Finland

(Received 21 June 2017; revised manuscript received 15 September 2017; published 30 October 2017)

In this study, thermal unpinning of edge dislocations from voids in α -Fe is investigated by means of molecular dynamics simulations. The activation energy as a function of shear stress and temperature is systematically determined. Simulations with a constant applied stress are compared with dynamic simulations with a constant strain rate. We found that a constant applied stress results in a temperature-dependent activation energy. The temperature dependence is attributed to the elastic softening of iron. If the stress is normalized with the softening of the specific shear modulus, the activation energy is shown to be temperature-independent. From the dynamic simulations, the activation energy as a function of critical shear stress was determined using previously developed methods. The results from the dynamic simulations are in good agreement with the constant stress simulations, after the normalization. This indicates that the computationally more efficient dynamic method can be used to obtain the activation energy as a function of stress and temperature. The obtained relation between stress, temperature, and activation energy can be used to introduce a stochastic unpinning event in larger-scale simulation methods, such as discrete dislocation dynamics.

DOI: [10.1103/PhysRevMaterials.1.053603](https://doi.org/10.1103/PhysRevMaterials.1.053603)

I. INTRODUCTION

Iron and iron-based alloys are the main choices for structural material due to their good mechanical properties. The mechanical properties can be enhanced by inserting alloying elements, precipitates, or in some other way changing the nanostructure of the material. The key mechanism behind the mechanical properties of materials is the motion of dislocations. Nanostructures are known to affect the movement of dislocations [1,2]. Hence, nanosized inclusions will ultimately affect the macroscopic behavior of the materials. Computer simulations provide a good tool for studying the interactions of dislocations with different nanosized obstacles at the atomic level [3–11]. Atomistic simulations are capable of simulating both the matrix material as well as the effect of alloying elements [3,4], coherent obstacles [5,6], and noncoherent obstacles [7–9].

Different types of steel are used as structural materials and for the reactor vessel in nuclear power plants, where they are exposed to continuous irradiation. It is known that irradiation will introduce point defects, dislocations, precipitates, and voids in the materials [12]. The structure and formation of the different defect clusters produced by irradiation can be studied in detail in atomistic simulations and compared with experiments [13,14]. Voids and other defect clusters can hinder the movement of dislocations in the material. Molecular dynamics (MD) simulations have previously been carried out extensively to study the interactions of both screw and edge dislocations with different sizes of voids in iron [3,5,10,11]. Typically, the dislocation-obstacle interactions are studied by applying a constant shear strain rate on the simulation system. From these dynamic simulations, the stress required for a dislocation to unpin from an obstacle can be determined. The unpinning stresses have been determined for

a wide range of temperatures, strain rates, and void sizes. Even though dynamic simulations in MD are a valuable way of investigating the atomistic interactions of dislocations with obstacles, the strain rates employed are (for computational reasons) usually extremely high compared to experiments. The stochastic behavior of a dislocation unpinning from an obstacle, due to thermal activation, is therefore underestimated or completely neglected.

Larger-scale simulation methods, like (discrete) dislocation dynamics, can be used to simulate lower strain rates, and to model systems larger than those computationally accessible in MD [15]. These methods rely on parameters from MD and experiments, such as the elastic moduli and the strengths of different obstacles. Dislocation dynamics simulations are able to describe the interactions between dislocations [15] as well as the interactions of dislocations with other defects and precipitates [16]. Even though MD simulations will give the critical unpinning stress for a certain sized obstacle at a certain temperature, the stochasticity of the unpinning event is usually not captured. The stochastic element of dislocation-obstacle interactions can be implemented in dislocation dynamics simulations as a probability of unpinning based on the activation energy associated with the obstacle, as a function of stress and temperature [17]. Monnet *et al.* proposed a method for determining the activation energy as a function of a derived critical stress from dynamic MD simulations [18]. To calculate the activation energy and critical stresses, the attempt frequency and activation volume for the dislocation pinned to the obstacle must be known. The former is usually taken as an order of magnitude parameter, and the latter is estimated based on the geometry of the pinned dislocation and obstacle.

In this article, we study in detail the thermal activation of an edge dislocation unpinning from a void in bcc Fe. The simulations are performed in a static (constant applied stress) situation at elevated temperatures to eliminate the strain rate dependence and capture the stochastic unpinning event. From the obtained results, we can estimate both the attempt frequency and the activation volume for the 2 nm void.

*Author to whom all correspondence should be addressed: jesper.byggmastar@helsinki.fi

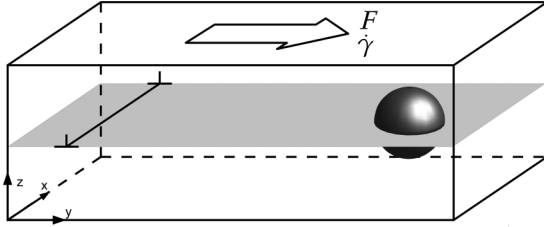


FIG. 1. Illustration of the simulation system with an edge dislocation moving toward a void as a result of an applied shear force F or shear strain rate $\dot{\gamma}$.

Simulations are performed at different temperatures and different constant stresses to obtain the dependence of both temperature and stress on the activation energy. Additionally, in order to extend the investigated stress and temperature range, the method by Monnet *et al.* was utilized in dynamic simulations [18] and compared with the results from static simulations.

II. METHODS

A. Molecular dynamics simulations

All simulations were carried out using the classical MD code PARCAS [19,20] with the embedded-atom method (EAM) potential by Ackland *et al.* [21]. The size of the simulation box containing the $1/2[111]$ edge dislocation and a 2 nm void was about $21 \times 25 \times 12 \text{ nm}^3$. The system was scaled to the correct lattice constant at each temperature. The x axis of the simulation system was oriented along the $[11\bar{2}]$ direction, the y axis along the $[111]$ direction, and the z axis along the $[1\bar{1}0]$ direction. Periodic boundary conditions were used in the x and y directions. A few of the top and bottom layers were kept fixed. The shear force was applied on the top layers of atoms. The simulation system is illustrated in Fig. 1 and the methods correspond to the model by Osetsky *et al.* for dislocation-obstacle simulations [22].

In the constant stress simulations (also referred to as the static simulations), the simulation scheme was as follows. The distance traveled as a function of time, separated into different stages of the simulation in a typical case, is shown in Fig. 2. During the first 10 ps (region A), the entire system was heated up and equilibrated at the desired temperature using the Berendsen temperature control [23]. During the next 20 ps (region B), a linearly increasing shear force was applied on a few of the top layers. The temperature control was then also turned off to avoid unphysical velocity scaling of the atoms and to allow for a natural thermal activation of the unpinning event. In region B the dislocation started moving in the y direction, but it did not reach the void to affect the measured activation time. At 30 ps, the shear force reached the value corresponding to the desired shear stress, and from thereon (region C) it was kept constant. At the point P in Fig. 2, the dislocation was pinned by the void. After the pinning point (region D), the probability of unpinning is determined purely by thermal activation at the given constant applied stress and temperature. The dislocation unpinned from the void at point U . After the unpinning (region E), the dislocation continued to move through the lattice past the void, and the simulation was stopped. The energy added to the system

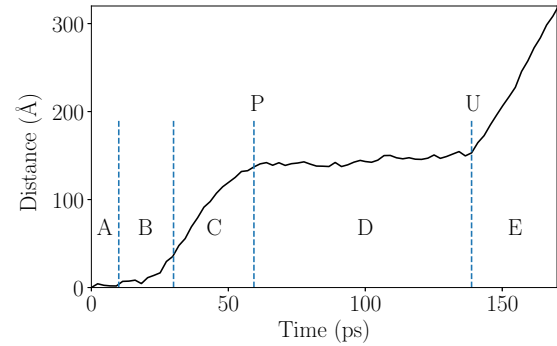


FIG. 2. The different stages during a constant stress simulation, illustrated as the distance traveled by the dislocation as a function of time in a typical case. Points P and U represent the pinning and unpinning of the dislocation. For a description of regions A–E, see the text.

through the applied shear force did not significantly raise the temperature. The requirement of relatively short unpinning times, due to computational efficiency, limited the studied applied stress interval to 180–205 MPa with temperatures in the range 650–1000 K. The mean activation time was obtained by averaging the activation times of 50 individual simulations at each stress-temperature pair.

Dynamic simulations were carried out in an extended temperature range (10–1000 K) with two different strain rates, 10^7 s^{-1} and $5 \times 10^6 \text{ s}^{-1}$. The strain rates correspond to dislocation velocities v of around 5 and 10 m/s through the Orowan equation $\dot{\gamma} = b\rho v$, where ρ is the dislocation density and b is the length of the Burgers vector. Border cooling was applied on a few layers of atoms above the fixed atoms at the bottom to keep the temperature constant. At each temperature, three simulations were carried out in order to assess the statistical variations. Additionally, we investigated the effect of the height of the dislocation glide plane with respect to the void using dynamic simulations. Three intersection heights were simulated, one that results in the dislocation gliding along the uppermost hollow plane of the void, and two intermediate heights between the top and center of the void.

B. Analysis and theoretical background

In the constant stress simulations, the time elapsed between the pinning and thermally activated unpinning of the dislocation, i.e., the activation time, was extracted by monitoring the dislocation velocity. The dislocation was defined as pinned to the void when its velocity dropped to below a certain threshold (0.1 nm/ps), and unpinned when the velocity reached 0.2 nm/ps (see Fig. 2). The validity of the chosen critical threshold velocities was confirmed by visual inspection. The position of the dislocation as a function of time was calculated by isolating the dislocation using the common neighbor analysis method implemented in OVITO [24].

Assuming the thermally activated unpinning of the dislocation follows an Arrhenius behavior, the rate of unpinning is given by

$$\frac{1}{\langle t_a \rangle} = \nu \exp\left(-\frac{E_a}{k_B T}\right), \quad (1)$$

where $\langle t_a \rangle$ is the mean activation time extracted from simulations at a given applied stress and temperature. k_B is the Boltzmann constant, T is the temperature, E_a is the activation energy, and ν is an attempt frequency associated with the event. The activation energy and attempt frequency can be estimated by fitting Eq. (1) to measured rates of activation at different temperatures in an Arrhenius plot. With a known estimate of the attempt frequency, the activation energy is given by rearranging Eq. (1) as

$$E_a = k_B T \ln(\nu \langle t_a \rangle). \quad (2)$$

The dislocation moves as a result of an externally applied shear stress. The stress is more appropriately given in terms of an effective stress on the obstacle due to the pinned dislocation [18], given by

$$\tau_{\text{eff}} = \left(1 + \frac{L-D}{D}\right) \tau_{\text{appl}} - \frac{L-D}{D} \tau_f. \quad (3)$$

Here, L is the obstacle spacing in the row of obstacles, and D is an activation length given by the missing segment of the pinned dislocation. Here, we use $D = 20 \text{ \AA}$, i.e., the approximate diameter of the void. τ_f is the stress required for the dislocation to move through the lattice (friction stress), which in this case is negligible.

For dynamic simulations, the activation time is directly dependent on the chosen strain rate. The concept of critical stress was introduced by Monnet *et al.* [18,25] as the effective stress averaged over a given stress history in the activation period, according to

$$\tau_C = \frac{k_B T}{V_a} \ln \left\langle \exp \left(\frac{V_a \tau_{\text{eff}}}{k_B T} \right) \right\rangle_{t_a}, \quad (4)$$

where V_a is an activation volume. The activation energy corresponding to the activation time can therefore be evaluated as a function of the critical stress at a given temperature. In the case of constant applied stress, τ_C is simply equal to τ_{eff} .

For stresses relatively close to the critical unpinning stress, the stress dependence of the activation energy of dislocation unpinning typically follows an equation in the form [26]

$$E_a = E_0 \left[1 - \left(\frac{\tau}{\tau_0} \right)^q \right]^p. \quad (5)$$

E_0 is a limiting energy parameter at $\tau = 0$, which is not necessarily equal to the total mechanical energy barrier, as the model is not accurate at very low stresses. τ_0 is the critical stress at 0 K, and the parameters p and q depend on the stress profile of the obstacle close to the critical stress. In the original derivation by Mott and Nabarro, $q = 1$ and $p = 3/2$ [27]. However, other choices for the functional form of the stress profile lead to other values of q and p [28]. In this work, instead of relying on a choice of shape of the stress profile, we keep $q = 1$ fixed and use p as a fitting parameter.

III. RESULTS

Assuming that the total energy barrier associated with a dislocation pinned to an obstacle is independent of temperature, given constant mechanical work on the dislocation, the remaining energy required by thermal activation is also

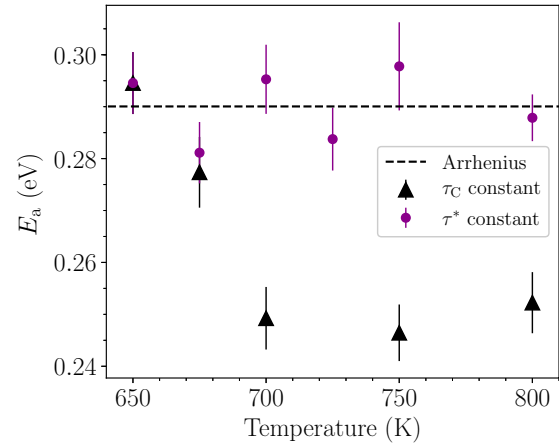


FIG. 3. Activation energy as a function of temperature from simulations with constant τ_C (constant applied stress) and constant τ^* . The error bars correspond to the standard errors of the mean activation times.

temperature-independent. However, as the mechanical work is provided in the form of an applied shear stress, the temperature dependence of the elasticity of the material will result in a temperature-dependent amount of work done on the system. We found that the softening of iron at higher temperatures results in an increase in the supplied mechanical work that cannot be neglected. As a good approximation, the shear softening can be accounted for by normalizing the critical stress as

$$\tau^* = \frac{G_0}{G(T)} \tau_C, \quad (6)$$

where $G(T)$ is the specific shear modulus of the system at temperature T , and $G_0 = G(T = 0)$. The values of G at different temperatures are given in Appendix A.

Figure 3 shows the activation energy in the temperature interval studied with a constant applied stress. The figure illustrates the need to account for the elastic softening of iron as the temperature is increased. With a constant applied stress at different temperatures, the measured activation energy is clearly temperature-dependent. Accounting for the temperature dependence of the shear modulus of the system

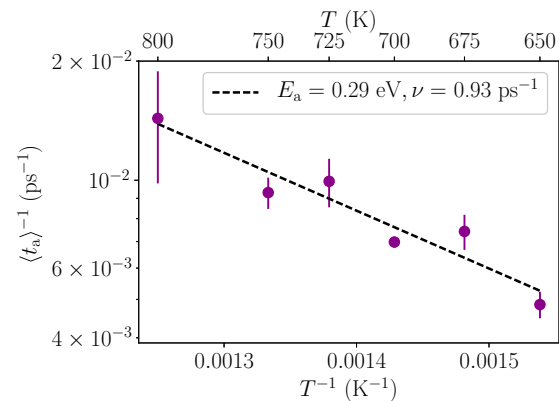


FIG. 4. Arrhenius plot to determine an average activation energy and attempt frequency from the simulations with constant τ^* .

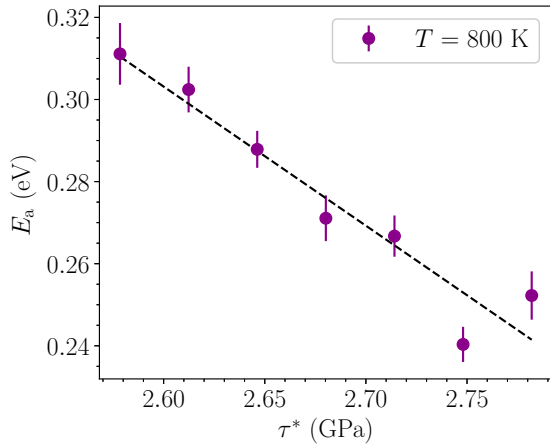


FIG. 5. Activation energy as a function of stress at constant temperature (800 K).

according to Eq. (6), and carrying out simulations with a constant τ^* , results in a (within the statistical uncertainty) temperature-independent barrier. Using the obtained average activation times, the activation energy and attempt frequency at a constant τ^* can be determined in an Arrhenius plot, shown in Fig. 4. The fitted Arrhenius line is also plotted in Fig. 3. The obtained value of 0.93 ps^{-1} for the attempt frequency is used in all calculations of the activation energy.

Figure 5 shows the stress dependence of the activation energy in the measured stress interval at constant temperature (800 K). The behavior is, to a good approximation, linear. The discrepancy of the last two (high stress) points from the linear relationship is due to the unpinning times becoming too small to be described by an Arrhenius behavior. This can be illustrated by the cumulative unpinning probability as a function of time, as seen in Appendix B. Accounting for the shear softening, all simulations with a constant applied stress can be shown to follow a similar linear behavior as a function of τ^* in the studied stress interval. Figure 6 shows all data obtained from the constant stress simulations. An approximate value for the activation volume can be obtained as the slope of the linear fit according to $E_a = E_0 - V_a \tau^*$ [18]. The obtained

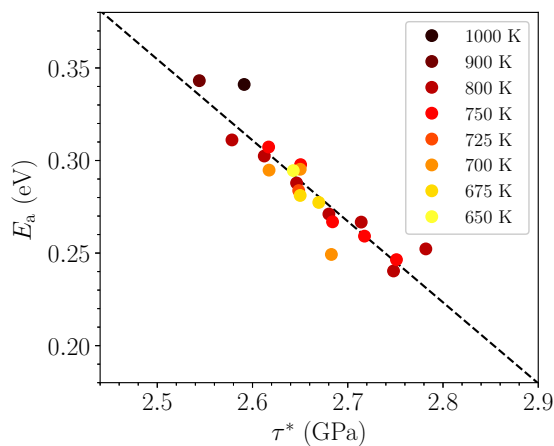


FIG. 6. Activation energy as a function of τ^* at different temperatures.

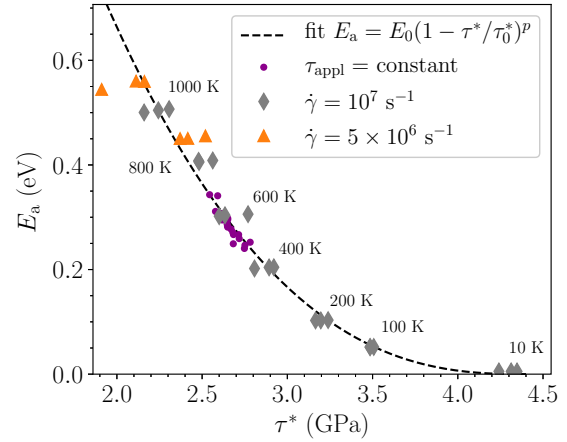


FIG. 7. Combined data for statically ($\tau_{\text{appl}} = \text{const}$) and dynamically calculated activation energies as a function of τ^* . The data follow Eq. (5) with $\tau_0^* = 4.4 \text{ GPa}$, $E_0 = 3.142 \text{ eV}$, and $p = 2.566$.

activation volume is $V_a = 70.1 \text{ \AA}^3$ and is used in the calculation of the critical stresses in the dynamic simulations.

Figure 7 shows the results of the dynamic simulations, where the critical stresses τ^* were calculated according to Eqs. (4) and (6). The results are combined with the data obtained from the constant stress simulations (Fig. 6) and fitted to Eq. (5). τ_0 was kept fixed to 4.4 GPa, a value slightly above the unpinning stress of the 10 K dynamic simulations. The obtained fit follows Eq. (5) with $E_0 = 3.142$ and $p = 2.566$.

The effect of the elastic softening on the activation energy at different temperatures can be illustrated by the fitted Eq. (5) as a function of the unnormalized critical stress τ_C . Figure 8 shows the activation energy as a function of τ_C , with Eq. (5) plotted at different temperatures using Eq. (6). From the figure it is clear that the temperature effect is significant and should therefore be accounted for using the softening of the specific shear modulus.

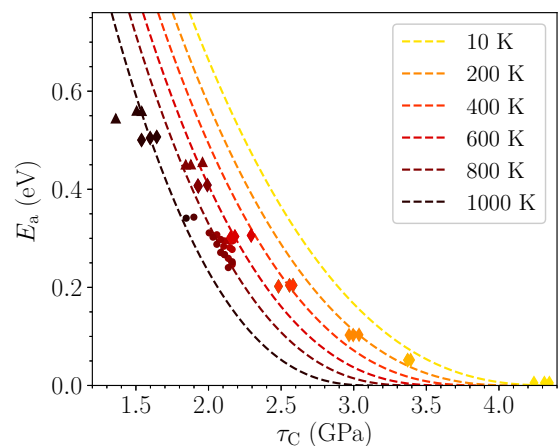


FIG. 8. The stress dependence (in terms of τ_C) of the activation energy at different temperatures, given by the fit to Eq. (5) in Fig. 7. The circles are the results from static simulations, the triangles are results from dynamic simulations at the lower investigated strain rate, and the diamonds are from the simulations with the higher strain rate.

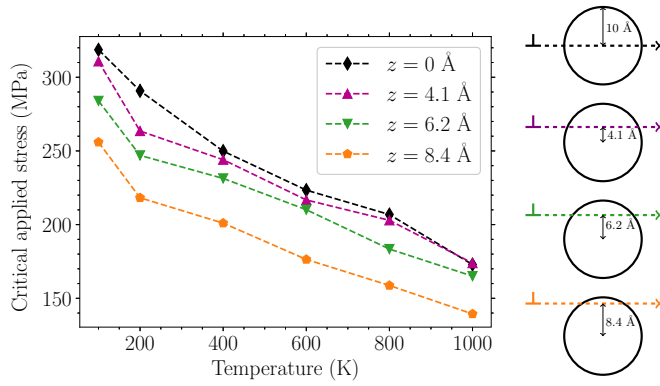


FIG. 9. Unpinning stress as a function of temperature for different void intersection heights (left) and illustrations of the void intersection heights (right). Each stress value is the average of three simulations.

Figures 9 and 10 show the results from the simulations at different void intersection heights. The critical applied stress required for the dislocation to unpin at different intersection heights, as a function of temperature, is given in Fig. 9. The intersection heights relative to the void are also illustrated. Figure 10 shows the calculated activation energies as a function the normalized stress τ^* . The activation volume, length, and the attempt frequency obtained in the static simulations were used when determining the critical stress and activation energy, but scaled according to the new pinning geometry of the void intersection. The new activation lengths were calculated with the assumption that the void is a perfect sphere, and they are 18.26 Å for $z = 4.1$ Å, 15.63 Å for $z = 6.2$ Å, and 10.85 Å for $z = 8.4$ Å. The last height corresponds to the dislocation passing through the uppermost hollow plane of the void. The scaled attempt frequencies and activation volumes for the different intersection heights are $\nu = 1.02$, 1.19, and 1.71 ps^{-1} , and $V_a = 64.0$, 54.8, and 38.0 Å³ for the given heights, respectively. However, it is worth noting that the frequency and volume dependencies in Eqs. (2) and (4) are weak, and the data shown in Fig. 10 are therefore not sensitive to the exact values of ν and V_a . The parameters

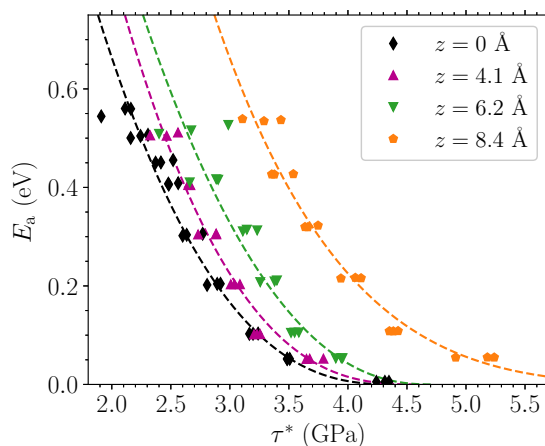


FIG. 10. Activation energies as functions of normalized stress τ^* for the different void intersection heights given by the dynamic simulations. The dashed lines are fits to Eq. (5).

for the fits to the Mott-Nabarro-like Eq. (5) are $E_0 = 4.0$ eV, $p = 2.73$ for $z = 4.1$ Å; $E_0 = 3.4$ eV, $p = 2.3$ for $z = 6.2$ Å; and $E_0 = 6.4$ eV, $p = 4.83$ for $z = 8.4$ Å. The corresponding 0 K critical stresses, τ_0 , are 4.6, 4.7, and 8.0 GPa.

IV. DISCUSSION

The static MD simulations allowed us to directly obtain values for the activation energy at independently chosen temperatures and applied stress values. However, due to the limited available time scale in MD, the temperature and stress ranges computationally available are fairly limited. Some important parameters can nonetheless be extracted and compared with theoretical estimations, and further used in dynamical MD simulations. We found that the attempt frequency, ν , close to the interface of the void is approximately 0.93 ps^{-1} . The attempt frequency is usually taken as an order of magnitude estimate, typically based on the Debye frequency scaled by the activation length l (i.e., the length of the missing segment of the pinned dislocation), and the length of the Burgers vector according to $\nu \approx \nu_D b/l$. Monnet *et al.* took the lower frequency at the interface of a void into account and used an attempt frequency equal to $\nu_D b/2l$ [18]. For a 2 nm void in iron, this results in attempt frequencies in the range 0.5–0.8 ps^{-1} (depending on the exact activation length), in good agreement with the value obtained directly from the static MD simulations in this study.

By assuming that the activation volume can be obtained approximately as the slope of the linear region in the stress dependence of the activation energy, we obtained a value of 70.1 Å³. As a simpler estimate, the activation can be assumed to be roughly equal to the volume spanned by the activation length at the void interface and the Burgers vector according to $V_a = lb^2$ [18]. Depending on the activation length, this results in volumes in the range 90–125 Å³, in reasonable agreement with the value estimated from the static MD data. The agreement between the attempt frequency and activation volume obtained from MD and values estimated by simple arguments, suggest that the latter can be used to obtain sufficiently good approximations when measured data are not available.

From the static MD simulations, we found that the increased applied mechanical work due to the softening of the specific shear modulus drastically change the activation energy at different temperatures, with a given applied shear stress. By accounting for the shear softening according to Eq. (6), the activation energy becomes independent of temperature, as is generally expected and often assumed. The effect of shear softening on the activation energies is easily obscured in dynamic simulations with high strain rates, and has therefore been ignored or neglected in earlier studies. Our results show the importance of accounting for the elastic softening when determining activation energies at different temperatures. Furthermore, as the EAM potential cannot reproduce the temperature dependence of the elastic constants at high temperatures (see Appendix A), the shear softening effect on the activation energy is likely even more pronounced than observed here.

Dynamic simulations are necessary to extend the limited stress and temperature ranges possible in static simulations, and determine a general form of the stress dependence of the activation energy. Using the information obtained from the static simulations along with the methods derived by Monnet *et al.* [18,25], the static results are found to be in good agreement with the dynamic results and follow a trend similar to earlier studies of dislocation-obstacle interactions [17,18,29]. The good agreement between the dynamic and static simulations, provided that the elastic softening is accounted for, can be seen as a strong validation of the methods introduced by Monnet *et al.* Hence, dynamic simulations in combination with the concept of critical stress [Eqs. (4) and (6)] can be used to obtain a relationship between the activation energy and stress for a given obstacle, with a few parameters obtained from static simulations or theoretical estimations.

The obtained Mott-Nabarro-like equation for the stress dependence of activation energy can be used in larger scale simulation methods, such as dislocation dynamics. As illustrated in Fig. 8, however, accounting for the softening effect requires including an explicit dependence of the shear modulus at the desired temperature. Using the fitted Eq. (5) together with Eq. (6), the appropriate temperature-dependent form of the activation energy as a function of the critical stress (as plotted in Fig. 8) obtained in this study for a dislocation passing through the center of a void in iron is then

$$E_a(\tau_c, T) = E_0 \left(1 - \frac{G_0 \tau_c}{G(T) \tau_0} \right)^p, \quad \begin{aligned} E_0 &= 3.142 \text{ eV}, \\ p &= 2.566, \\ \tau_0 &= 4.4 \text{ GPa}, \end{aligned} \quad (7)$$

where G is the appropriate shear modulus for the shear system [see Appendix A for $G(T)$ of the system in this study]. The probability or rate of unpinning can then be directly determined and used in e.g. a dislocation dynamics simulation at any desired temperature.

Equation (7) is valid for an edge dislocation gliding through the center of a void. The effect of the intersection height relative to the obstacle on the critical unpinning stress was previously studied in detail for voids and Cu precipitates in iron [30]. We carried out dynamic simulations to study this effect on the activation energy function. The dependence on intersection height is relatively weak for a large part of the void cross section, but is significant when the dislocation passes very close to the top of the void. The different geometry for the dislocation pinned at the top of the void, with crystalline atoms above the dislocation line and the void below, are seen to affect the effective unpinning stresses, and the corresponding activation energy curve deviates strongly from the other intersection heights. Although we only studied positive intersection heights, i.e. when a smaller portion of the extra atomic plane passes through the void, earlier studies found the effects to be also similar for negative intersection heights [30].

V. CONCLUSIONS

We have carried out molecular dynamics simulations of an edge dislocation unpinning from a 2 nm void in α -Fe by thermal activation. The activation energy as a function of applied stress and temperature was systematically determined

by applying a constant shear stress and measuring the activation time. We found that the increased supplied mechanical work due to shear softening of iron at higher temperatures results in a non-negligible temperature dependence of the activation energy. The temperature dependence is found to be largely due to the temperature dependence of the specific shear modulus.

Dynamic simulations with a constant shear strain rate were carried out over an extended stress and temperature range. The activation energy as a function of the critical stress was determined using earlier derived methods. The results from dynamic simulations were found to be in good agreement with the static simulations, provided that the shear softening is accounted for. The obtained relation between activation energy and critical stress can be used in larger-scale simulation methods, such as dislocation dynamics. The methods used here should be applicable to other types of obstacles, and provide a framework for systematically obtaining the activation energy as a function of stress and temperature for any given obstacle.

ACKNOWLEDGMENTS

This work has been carried out within the framework of the EUROfusion Consortium, and it received funding from the Euratom research and training programme 2014-2018 under Grant Agreement No. 633053. The views and opinions expressed herein do not necessarily reflect those of the European Commission. The authors wish to acknowledge CSC-IT Center for Science, Finland, for computational resources.

APPENDIX A: TEMPERATURE DEPENDENCE OF THE SPECIFIC SHEAR MODULUS $G(T)$

Figure 11 shows the temperature dependence of the specific shear modulus of α -Fe in the EAM potential by Ackland *et al.* [21]. The shearing direction is [111] (y axis in Fig. 1) and the shear plane [1 $\bar{1}$ 0] (z axis), with the [11 $\bar{2}$] direction along the x axis. Each point is an average of three separate simulations. The data are well described by the linear equation $G(T) = aT + G_0$, with $a = -0.0203$ GPa/K and $G_0 = 71.3$ GPa. The simulation results are compared with experimental data

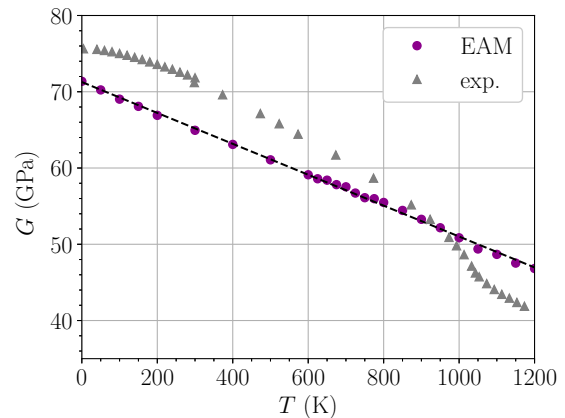


FIG. 11. Temperature dependence of the specific shear modulus in the [111] direction calculated with the potential by Ackland *et al.* [21] and compared with experimental data [33,34].

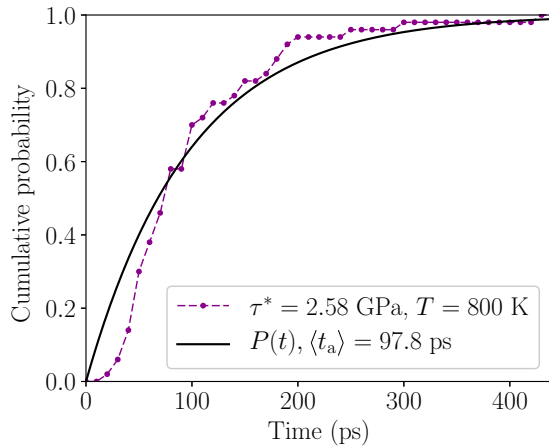


FIG. 12. Cumulative probability of unpinning as a function of time according to Eq. (B1) at 800 K.

calculated using the temperature dependence of the elastic constants c_{ij} . The relation between the elastic constants and the specific shear modulus for a $\langle 111 \rangle$ direction is $G = (c_{11} - c_{12} + c_{44})/3$ [31,32]. The experimental data for the temperature dependence of the elastic constants are taken from Refs. [33] and [34]. The increased temperature dependence at around 800 K and above is attributed to the loss of magnetic order close to the Curie temperature [34], an effect the EAM potential cannot reproduce.

APPENDIX B: CUMULATIVE PROBABILITY OF UNPINNING

Given an Arrhenius behavior, the cumulative probability of activation (unpinning) as a function of time is expected to

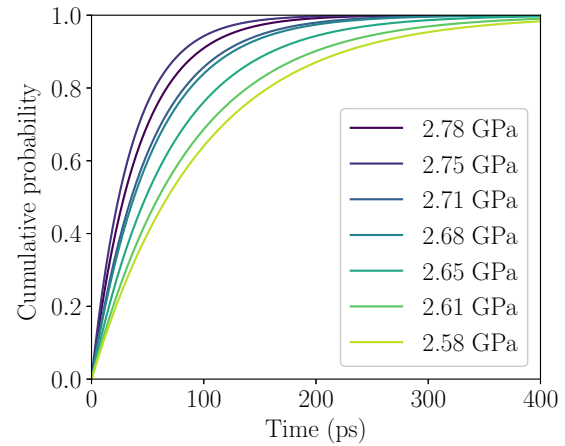


FIG. 13. Cumulative probability of unpinning as a function of time according to Eq. (B1) at 800 K and different critical stresses τ^* .

follow the exponential cumulative distribution

$$P(t) = 1 - \exp\left(-\frac{t}{\langle t_a \rangle}\right). \quad (\text{B1})$$

The simulated cumulative probability distribution at a constant applied stress can be directly compared with the expected distribution. Figure 12 shows an example of the measured cumulative probability and the corresponding exponential distribution using the calculated mean activation time in Eq. (B1). The measured probability of unpinning follows the expected distribution, except at very low times. Figure 13 shows the cumulative distributions for all critical stresses at 800 K using the corresponding mean activation times.

-
- [1] J. P. Hirth and J. Lothe, *Theory of Dislocations*, 2nd ed. (Krieger, Malabar, 1992).
- [2] W. D. Callister, *Materials Science and Engineering: An Introduction*, 3rd ed. (Wiley, New York, 1993).
- [3] R. Schäublin and S. M. Hafez Haghghat, *J. Nucl. Mater.* **442**, S643 (2013).
- [4] S. Schmauder and C. Kohler, *Comput. Mater. Sci.* **50**, 1238 (2011).
- [5] Y. N. Osetsky and D. J. Bacon, *J. Nucl. Mater.* **323**, 268 (2003).
- [6] D. A. Terentyev, G. Bonny, and L. Malerba, *Acta Mater.* **56**, 3229 (2008).
- [7] F. Granberg, D. Terentyev, K. O. E. Henriksson, F. Djurabekova, and K. Nordlund, *Fusion Sci. Technol.* **66**, 283 (2014).
- [8] F. Granberg, D. Terentyev, and K. Nordlund, *J. Nucl. Mater.* **460**, 23 (2015).
- [9] F. Granberg, D. Terentyev, and K. Nordlund, *Nucl. Instrum. Methods Phys. Res. Sec. B* **352**, 77 (2015).
- [10] D. Terentyev, D. J. Bacon, and Y. N. Osetsky, *J. Phys.: Condens. Matter* **20**, 445007 (2008).
- [11] S. M. Hafez Haghghat, J. Fikar, and R. Schäublin, *J. Nucl. Mater.* **382**, 147 (2008).
- [12] Z. Yao, M. L. Jenkins, M. Hernández-Mayoral, and M. A. Kirk, *Philos. Mag.* **90**, 4623 (2010).
- [13] R. E. Stoller, *Comprehensive Nuclear Materials* (Elsevier, Oxford, 2012), p. 293.
- [14] L. Malerba, *J. Nucl. Mater.* **351**, 28 (2006).
- [15] V. Bulatov and W. Cai, *Computer Simulations of Dislocations*, 1st ed. (Oxford University Press, Oxford, 2006).
- [16] A. Lehtinen, F. Granberg, L. Laurson, K. Nordlund, and M. J. Alava, *Phys. Rev. E* **93**, 013309 (2016).
- [17] D. Terentyev, G. Monnet, and P. Grigorev, *Scr. Mater.* **69**, 578 (2013).
- [18] G. Monnet, Y. N. Osetsky, and D. J. Bacon, *Philos. Mag.* **90**, 1001 (2010).
- [19] K. Nordlund, M. Ghaly, R. S. Averback, M. Caturla, T. Diaz de la Rubia, and J. Tarus, *Phys. Rev. B* **57**, 7556 (1998).
- [20] M. Ghaly, K. Nordlund, and R. S. Averback, *Philos. Mag. A* **79**, 795 (1999).
- [21] G. J. Ackland, M. I. Mendelev, D. J. Srolovitz, S. Han, and A. V. Barashev, *J. Phys.: Condens. Matter* **16**, S2629 (2004).
- [22] Y. N. Osetsky and D. J. Bacon, *Modell. Simul. Mater. Sci. Eng.* **11**, 427 (2003).
- [23] H. J. C. Berendsen, J. P. M. Postma, W. F. v. Gunsteren, A. DiNola, and J. R. Haak, *J. Chem. Phys.* **81**, 3684 (1984).
- [24] A. Stukowski, *Modell. Simul. Mater. Sci. Eng.* **18**, 015012 (2010).

- [25] C. Domain and G. Monnet, *Phys. Rev. Lett.* **95**, 215506 (2005).
- [26] U. F. Kocks, A. S. Argon, and M. F. Ashby, *Thermodynamics and Kinetics of Slip* (Pergamon Press, Oxford, 1975).
- [27] N. F. Mott and F. R. N. Nabarro, Physical Society Bristol Conference Report (1948), p. 1.
- [28] G. B. Gibbs, *Mater. Sci. Eng.* **4**, 313 (1969).
- [29] G. Bonny, D. Terentyev, J. Elena, A. Zinovev, B. Minov, and E. E. Zhurkin, *J. Nucl. Mater.* **473**, 283 (2016).
- [30] P. Grammatikopoulos, D. J. Bacon, and Y. N. Osetsky, *Modell. Simul. Mater. Sci. Eng.* **19**, 015004 (2011).
- [31] P. Heino, H. Häkkinen, and K. Kaski, *Europhys. Lett.* **41**, 273 (1998).
- [32] K. M. Knowles and P. R. Howie, *J. Elast.* **120**, 87 (2015).
- [33] J. A. Rayne and B. S. Chandrasekhar, *Phys. Rev.* **122**, 1714 (1961).
- [34] D. J. Dever, *J. Appl. Phys.* **43**, 3293 (1972).